APPLIED GEOPHYSICS, Vol.15, No.3–4 (September–December 2018), P. 524–535, 8 Figures.
DOI:10.1007/s11770-018-0688-3

Three-dimensional gravity inversion based on sparse recovery iteration using approximate zero norm*

Meng Zhao-Hai♦[1, 4], Xu Xue-Chun[2], and Huang Da-Nian[3]

Abstract: This research proposes a novel three-dimensional gravity inversion based on sparse recovery in compress sensing. Zero norm is selected as the objective function, which is then iteratively solved by the approximate zero norm solution. The inversion approach mainly employs forward modeling; a depth weight function is introduced into the objective function of the zero norms. Sparse inversion results are obtained by the corresponding optimal mathematical method. To achieve the practical geophysical and geological significance of the results, penalty function is applied to constrain the density values. Results obtained by proposed provide clear boundary depth and density contrast distribution information. The method's accuracy, validity, and reliability are verified by comparing its results with those of synthetic models. To further explain its reliability, a practical gravity data is obtained for a region in Texas, USA is applied. Inversion results for this region are compared with those of previous studies, including a research of logging data in the same area. The depth of salt dome obtained by the inversion method is 4.2 km, which is in good agreement with the 4.4 km value from the logging data. From this, the practicality of the inversion method is also validated.
Keywords: Three-dimensional gravity inversion, sparse recovery, approximate zero norm, iterative method, density constraint penalty function

Introduction

Geophysicists expect much geological information from gravity data; therefore, precise relay and interpretation of these data is crucial. The proposed three-dimensional (3D) gravity inversion can quantitatively describe sub-surface density distribution characteristics; nevertheless, it is faced with several challenging, key problems: 1. It provides a two-dimensional (2D) surface gravity information of a sub-surface anomaly, which is difficult to process for 3D density distribution outputs; 2. There is equivalence of gravity field data, meaning, sub-surface anomalies of different volumes gives the same gravity data, leading to multiple solutions of inversion results, and; 3. There is volume effect of gravity field data, meaning, each observed gravity data point is the comprehensive reaction of the sub-surface anomalies; hence, obtaining sub-surface anomaly information from the surface gravity data is difficult. For the reasons cited,

Manuscript received by the Editor November 7, 2017; revised manuscript received October 28, 2018.
*This work was supported by the Development of airborne gravity gradiometer (No. 2017YFC0601601) and open subject of Key Laboratory of Petroleum Resources Research, Institute of Geology and Geophysics, Chinese Academy of Sciences (No. KLOR2018-8).
1. Tianjin Navigation Instrument Research Institute, Tianjin 300131, China.
2. College of Earth Sciences, Jilin University, Changchun 130021, China.
3. College of Instrumentation and Electrical Engineering, Jilin University, Changchun 130021 China.
4. Key Laboratory of Petroleum Resources Research, Institute of Geology and Geophysics, Chinese Academy of Sciences, Beijing 100029, China.
♦Corresponding author: Meng Zhao-Hai (Email: 526468457@qq.com)
© 2018 The Editorial Department of **APPLIED GEOPHYSICS.** All rights reserved.

the 3D gravity data inversion results are unstable and non-unique (Blakely, 1996).

Geophysicists have applied the constantly improving mathematical algorithms to solve the problems associated with the 3D gravity data inversion. Two methods were mainly used to solve the multiple solutions and instability of gravity data inversion. (1) The first method is direct inversion. Here fitting analysis between data calculated by the forward models and inversion results are studied, and the geological information are applied in the inversion research. Afterwards, sub-surface geological anomalies with relatively shallow depth and complicated geometry are interpreted by a human-computer interactive inversion method; thus, the accuracy of inversion results is mainly determined by the interpreter's understanding. (2) The inversion employs mathematical optimization to find the optimal solution of linear or non-linear functions (Gholami and Siahkoohi, 2010; Bijani et al., 2015; Ghalehnoee et al., 2017; Zhang et al., 2018). The geometry, spatial location, and distributions of density contrast are obtained by this method. Several related approaches have been studied to obtain the density distribution of target anomalies, which are categorized into inversion methods using little prior information (Last and Kubik, 1983; Barbosa and Sliva, 1994; Li and Oldenburg, 1998; Porniaguine and Zhdanov, 1999; Bertete-Aguirre et al., 2002; Farquharson, 2008; Fregoso and Gallardo, 2009; Wang et al., 2017) and those using much prior information (Guillen and Menchetti, 1984; Silva et al., 2006; Lelievre and Oldenburg, 2009; Silva Dias et al., 2009; 2011).

The key technologies involve discretization of sub-surface domain to establish linear or non-linear relationship between gravity data and sub-surface density contrast distribution and to formulate a mathematical theory capable of solving the established objective equation and obtaining the sub-surface density distributions of anomalies (Gholami and Siahkoohi, 2010; Bijani et al., 2015; Ghalehnoee et al., 2017; Zhang et al., 2018). Qi et al. (2012) introduced prior geological information to establish a sub-surface three-dimensional gravity and magnetic models that would reduce the uncertainty of inversion results; however, this method is not suitable for regions that have insufficient geological information. To compensate for this weakness, the Tikonov regularization theory was introduced and added a number of mathematical constraints to reduce the instability and non-uniqueness of inversion results. For example, prior information was added into the model function in the form of weight function. Minimization of the target model and data misfit functions was then achieved using the constraint of model parameter function. Finally, theoretically optimal inversion results were obtained. Different constraints can be introduced simultaneously according to the fundamental characteristics of different potential field data to overcome their shortcomings (such as the convergence effect of forward kernel function in 3D gravity inversion). DeGroot-Hedlin and Constable (1990) discovered a constraint condition that overcomes potential field defect by studying the kernel function. Li and Oldenburg (1996, 1998) introduced this method into gravity data and magnetic data inversion. With the depth weighting function applied to counteract the attachment effect of gravity and magnetic field data, the inversion results obtained were in accordance with the actual geological conditions. Last and Kubik (1983) used an approach to minimize the volume of anomalies, and then compressed the volume of abnormal sources in a more reasonable range, to define the sharp density boundary of these anomalies. Subsequently, a large number of geophysicists have improved this principle, while constantly enhancing its efficiency and practicality (Guillen and Menichetti., 1984; Barbosa and Silva, 1994; Portniaguine and Zhdanov, 1999; Zhdanov et al., 2004; Commer, 2011). Another method, the focusing inversion, was applied by Totini et al. (2009, 2012) to the seafloor magnetic field data of New Zealand volcanic hydrothermal system in the South Pacific Ocean to analyze the variation characteristics of seafloor rock susceptibility, and to simultaneously obtain the accurate inversion results by introducing rock physical constraints into the inversion research of gravity field data. Afterwards, the non-linear relationship between observed data and anomalous bodies was established, which was then solved by mathematical models to obtain the final inversion results. Commer (2011) applied non-linear conjugate gradient method to solve gravity gradient inversion problems with weight function. Upper and lower limit density constraint functions were in the form of a global objective function that increases the accuracy of inversion results. These inversion methods plays an important role in the quantitative interpretation of gravity field data, as they are helpful in the study of geosciences, including establishment of geological models and restoration of sub-surface geological structures, among others.

The volume of sub-surface anomaly body is normally smaller than the whole sub-surface space, while its mesh is sparse. Taking these characteristics into account, this paper focuses on an inversion method that introduces the concept of zero norm function (the number of non-zero

elements) into the model objective function, in order to constrain the sub-surface model. Mathematical theory and model test prove that the zero norm constraint function can solve the instability and non-uniqueness of problems in 3D inversion to a certain extent. At the same time, solve the zero norm is rigorous and challenging. We use the function of approximate zero norm instead of zero norm to constrain the object, which is solved by iterative solution method, and determine the sub-surface density distribution characteristics of the study region. This inversion method is applied to the actual gravity data in Texas, USA.

Methods and principles

The forward theory of gravity data

Firstly, the sub-surface should be discretized, and the space is divided into several adjacent prims consisting of the subsurface space. The density of each unit should be stable. In the Cartesian coordinate system (Z-axis is vertically down, X- and Y-axes are horizontal), we define a coordinate origin O. Using Newton's law of universal gravitation, we could obtain the gravity potential field data. The residual gravity field caused by any point in the ground space is given by

$$\mathbf{U(r)} = \gamma \iiint_V \frac{\mathbf{m}}{\mathbf{r}} dV, \tag{1}$$

where **m** is the density contrast of the subsurface anomaly, **V** is the volume, **U(r)** is the gravitational field, γ is the gravitational constant, and **r** is the distance between the observation point and the anomalous source. Subsequently, the value of gravity anomaly is

$$\mathbf{g} = \frac{\partial \mathbf{U}}{\partial \mathbf{z}}, \tag{2}$$

where **U** is the gravity field.

The forward formulation of the sub-surface abnormal rectangular cell is obtained by equation (1) (Blakely, 1996)

$$g = \gamma m\{-(x-\xi)\ln[r+(y-\eta)] - (y-\eta)\ln[r+(x-\xi)] + (z-\zeta)\arctan\frac{(x-\xi)(y-\eta)}{(z-\zeta)r}\}\Big|_{\xi_1}^{\xi_2}\Big|_{\eta_1}^{\eta_2}\Big|_{\zeta_1}^{\zeta_2}, \tag{3}$$

where (x, y, z) is the coordinate of the observations, and (ξ, η, ζ) is the coordinates center of the subsurface anomalies such that

$$r = [(x-\xi)^2 + (y-\eta)^2 + (z-\zeta)^2]^{\frac{1}{2}}.$$

The gravity data on the ground is obtained according to the forward formula of rectangle bodies, which consist of each rectangular discrete anomalous subsurface space. Using the superposition principle for each gravity data of each prism results to the discrete gravity data formula (Li and Oldenburg, 1998)

$$\mathbf{d} = \mathbf{Gm}, \tag{4}$$

where $\mathbf{G} \in \mathbf{R}^{N \times M}$ represents the gravity forward kernel function of the density distribution model space, $\mathbf{m} \in \mathbf{R}^{M \times 1}$ is the subsurface space density distribution vector, and $\mathbf{d} \in \mathbf{R}^{N \times 1}$ is the surface observed gravity data. Here, *M* and *N* respectively represent the number of the subsurface space prism and the corresponding value of the observed gravity data points.

Principle of 3D gravity data inversion

Non-uniqueness and instability of gravity inversion is attributed to much less number of observation points than the number of discrete meshes in a sub-surface space. This leads to equation (4) usually being an underdetermined linear equation. We employ the sparse recovery iteration method based on zero norm to solve the underdetermined linear equation and obtain a relatively accurate inversion result. Zero norm sparse recovery has been widely applied in other geophysical data processing fields, such as gravity data re re-grid and seismic data quality restoration (Chen et al., 2013; Chen and Chen, 2014). In thus paper, the zero norm function is introduced into 3D gravity inversion.

Generally, the number of subsurface grid is *Nz* times than the number of ground gravity observation points (*Nz* is the number of the vertical layer), which is much larger than the number of ground observation points. In other words, in the underdetermined functions **d = Gm**, the number *M* of the unknown solution **m** is far greater than the number of *N* (the number of ground observation points) equations. Thus, these equations contain infinite solutions according to the mathematical theory. Because the number of anomalous bodies' prisms in the subsurface is sparse, the zero norm function of the model parameter is introduced to obtain the optimal inversion results, which are the most sparse inversion results. The objective function is based on the inverse problem of **d = Gm**, which can be transformed into one of the most sparse optimization problems

$$\begin{cases} \min & \left\| \mathbf{m} - \mathbf{m}_{\mathbf{pre}} \right\|_0 \\ s.t. & \mathbf{d} = \mathbf{Gm} \end{cases}, \tag{5}$$

where $\mathbf{m} = (m_1, m_2, \ldots, m_N)$ is the density contrast of the target anomalies relative to the surrounding rock, and $\mathbf{m}_{\mathbf{pre}} = (mpre_1, mpre_2, \ldots, mpre_N)$ is a priori density contrast of the target anomalies.

The proposed inversion method is based on the theory of sparse recovery, which demand solution using the reconstruction algorithm of zero norm minimization. Here, zero norm is defined as the number of non-zero vector elements. However, Li et al. (2003), and Tao (2005), and Donoho and David (2006) pointed out that the direct solution of equation (5) with the zero norm is very challenging to obtain, as this is classified as an N-P difficult mathematical problem. Therefore, it needs to be solved approximately by other mathematical methods. There are several main methods applicable in solving the problem of zero norms. Basis Pursit algorithm is an effective method (Chen et al., 1998; Li et al., 2003; Donoho, 2006), while Matching Pursuit is another fast algorithm (Mallat and Zhang, 1993; Gribonval and Lesage, 2006). The downside of these algorithms is they are greedy, where calculations could be very slow, aside from needing to enhance the accuracy of the sparse recovery. Therefore, based on full range search, these greedy algorithms are not suitable for large scale sparse recovery problems. Besides, a number of alternative methods using an L1 norm can be used to approximately replace the zero norms, such as the interior point, iterative weight weighted L1 norm, projection gradient, and so on (Chen et al., 2001; Elad, 2007; Figueiredo et al., 2007).

For this work, an approximate zero norm function replaces the zero norm to solve the occurrence of N-P hard problem for zero norms. The selected approximate function is a smooth Gauss function, in which the expected value is zero; this mathematical model is capable of solving the problem of zero norm (Mohimanni et al., 2009). In the case where regional geological data are inadequate, the prior density value $\mathbf{m}_{\mathbf{pre}}$ is to zero, then the inversion process begins. Here, the expression form of the approximate zero norm function is expressed as

$$f_\sigma(\mathbf{m}) = \exp\left(\frac{-\mathbf{m}^2}{2\sigma^2}\right), \tag{6}$$

where $\mathbf{m}$ is the residual density contrast, and σ is a parameter to control the degree of the smoothness and sharpness of $\boldsymbol{f}_\sigma(\mathbf{m})$. Subsequently,

$$\lim_{\sigma \to 0} f(m) = \begin{cases} 1 & m = 0 \\ 0 & m \neq 0 \end{cases}. \tag{7}$$

The approximate zero norms proposed in this part should be discrete,

$$F_\sigma(\mathbf{m}) = \sum_{i=1}^{N} f_\sigma(\mathbf{m}_i). \tag{8}$$

Moreover, M is the number of discrete subsurface spaces such that

$$\lim_{\sigma \to 0} \mathbf{F}_\sigma(\mathbf{m}) = M - \left\| \mathbf{m} \right\|_0. \tag{9}$$

Using Gauss approximation after discretization, the N-P hard problem in the process of zero norm solution can be solved well (Mohimani et al., 2009). Alternatively, M–$\mathbf{F}_\sigma(\mathbf{m})$ also approximates the zero norm of $\mathbf{m}$ such that

$$\left\| \mathbf{m} \right\|_0 \approx M - \mathbf{F}_\sigma(\mathbf{m}), \tag{10}$$

where there is a very essential parameter σ for the whole inversion method process.

The parameter σ plays a very significant role in the final solution of this problem, as it selects a value that determines the approximate degree of smoothness and an approximation of the function $\mathbf{F}_\sigma$. The smaller σ is, the more accurate the approximation is; likewise, the smoother the Gauss function selection is, the easier the true global minimum solution is.

Based on the analysis of formulations (9) and (10), a sufficiently small σ lets us discover that the minimum problem of $\mathbf{F}_\sigma(\mathbf{m})$ can be replaced by a maximum problem. In other words, the minimum problem can be transformed into another function form as determined by

$$\begin{cases} \mathbf{m} = \arg\max \mathbf{F}_\sigma(\mathbf{m}) \\ \mathbf{d} = \mathbf{Gm} \end{cases}. \tag{11}$$

Equation (11) can be simplified by an iterative method using two techniques: (1) descending sequence value of σ as outer iteration and (2) giving σ value as inner iteration to solve the equation.

We mainly use the Lagrange method to approach this problem. The Lagrange multiplier and functions are introduced in

$$\mathbf{L}(\mathbf{m}, \lambda) = \mathbf{F}_\sigma(\mathbf{m}) + \lambda^T(\mathbf{Gm} - \mathbf{d}). \tag{12}$$

The Karush–Kuhn–Tuchker system is ideal (Cheng,

2013) to solve equation (12),

$$\begin{aligned} \frac{\partial L}{\partial m_i} &= m_i \exp(-\frac{m_i^2}{2\sigma^2}) + (G^T \lambda_j) = 0, \quad i = 1, 2, ..., M \\ \frac{\partial L}{\partial \lambda_j} &= (Gm_i - d)_j = 0, \quad j = 1, 2, ..., N. \end{aligned} \quad (13)$$

We use an approximate method to deal with the inner iteration. Given the initial value of σ_0, $\mathbf{m}^{(0)}$ through n iteration to get the final error, meets the accuracy required of the results. Thus, we obtain

$$\begin{aligned} m_i^{n+1} \exp(-\frac{(m_i^{(n)})^2}{2\sigma_n^2}) + (G^T \lambda^{(n+1)})_i = 0, \quad i = 1, 2, ..., M \\ Gm_i^{(n+1)} - d_j = 0 \qquad\qquad j = 1, 2, ..., N. \end{aligned} \quad (14)$$

In the inversion process, selecting the value of σ is very crucial. If it is too large, then the resulting approximate degree of zero norm will not enough or too far, thus, reducing the inversion resolution as inversion results become over smooth. In contrast, if the choice is too small, the inversion solutions will easily fall into the local minimum solution trap, as well as easily get affected by the Gauss noise. σ does not only guarantee a global minimum solution or avoid the influence of noise, but also ensures the target function to approximate the zero norm so that an accurate inversion solution is produced. The decreasing sequence form are used as the external iteration for similar reasons. The updated parameters are obtained by

$$\sigma^{(n+1)} = \rho\sigma^{(n)}, \quad (15)$$

where ρ is usually between 0–1 to ensure that σ follows a decreasing sequence.

Formula deduction yields a new inversion weight function. Constantly updating this weight function enables the iteration inversion results to approximate the real subsurface model very well. The new weight function is expressed as

$$w^{(n)}{}_i = \frac{1}{1 - \exp(-\frac{(m^{(n)}{}_i)^2}{2\sigma^{(n)2}}) + 10^{-20}}, \quad (16)$$

where the appearance of 10^{-20} prevents the emergence of zero values in the vector **m**, which will make the function meaningless.

Following a series of formulas derivation below, a new inversion algorithm can be obtained.

1.The initial value of the inversion model density is set to $\mathbf{m} = \mathbf{0}$. The first iteration results are set as the true initial value $\mathbf{m}_0$ (the conjugate gradient method is used as the initial value), $\sigma^{(0)} = 100 \times \max(\mathrm{abs}(\mathbf{m}_0))$, and ρ=0.8.

2.The conjugate method is employed to obtain the inversion results $\mathbf{m}^{(n)}$, where n is the number of iterations. At the same time, the weight function matrix $\mathbf{W}^{(n)}$ is updated continuously. Matrix $\mathbf{W}^{(n)}$ is the diagonal matrix of the n×n order; its component in the diagonal is $1/wi^{(n)}$, and its value is continuously updated to a new function $\mathbf{w}(n)$, $\mathbf{wi}(n+1)=1\text{-}1/(\exp\text{-}(\mathbf{mi}(n)+1)^2/2(\sigma(n+1))^2)+10^{-20})$.

3. Parameter σ in the outer loop is updated to $\sigma^{(n+1)} = \rho\sigma^{(n)}$.

4. If $\sigma<10^{-8}$, then updating stops and this value is maintained. The stopping criteria for this inversion iteration of the new inversion method is

$$RMS = \frac{(\mathbf{d} - \mathbf{Gm})^T (\mathbf{d} - \mathbf{Gm})}{N} < 10^{-4}. \quad (17)$$

5. When the iterative stopping condition is satisfied, the output is taken as the final and most accurate result of the inversion.

Choice of parameters

The proposed algorithm has two important parameters σ and ρ, which greatly influence the accuracy and success of results obtained by the final recovery sparse inversion. Varying and selecting these values directly affect the accuracy of the results, along with the degree of noise influence. Figure 1 describes the influence of different ρ for the approximate zero norms. Through an analysis of the approximate zero norm and number of experiments conducted, we discover that the best ρ is between 0.5–1.0, as this selection can prevent the parameter falling too fast leading to unstable inversion results. In this paper, we choose ρ = 0.8. As mentioned previously. the initial value of σ determines the degree of quality of the final inversion results; a small σ may make the results fall into the local minimum, while a large σ may not only make the results too smooth to give an accurate restriction for the inversion, but will also raise the number of iterations. Therefore, we used an adaptive method to update σ in each iteration process by multiplying it with ρ, using twice the absolute value of the maximum density in the

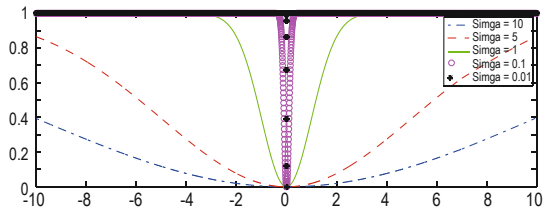

Fig. 1 Change characteristics of approximate zero norms with different ρ values.

initial iteration as the initial value ensuring the weight of the anomalous density body during the inversion. In mathematical theory, this parameter variation method ensures the convergence of the final inversion result.

Density contrast penalizes function

3D gravity data inversion aims to obtain the spatial distribution characteristics of the subsurface anomalies for a more comprehensive understanding of subsurface geological structure and mineral distribution characteristics. The sparse recovery method we adopted can basically solve the problem of gravity 3D inversion and obtain the 3D density distribution characteristics of the relatively accurate subsurface anomaly sources. However, to obtain the 3D inversion results with more realistic physical and geological meaning, the density contrast from the inversion should be constrained in real and accurate range. The density constraint function selection method is described in the following. A subsurface inversion space consists mainly of two density models, namely, rock density and anomaly. In the inversion, the surrounding rock density is the inversion density standard, thus, we can think of it as a density of a surrounding rock with a zero residual value. The density contrast of target anomalous bodies refers to the difference between the density of the anomalous bodies and the density of the surrounding rock. Based on the geological data of the inversion region, the average density of the surrounding rock can be found, and the observed gravity potential field data are processed to remove the anomalies caused by the regional density. Simultaneously, using the geological data to determine the density change in the anomalous sources, we can pinpoint the limitation of the anomalous density, and then contrast the inversion results in a reasonable density range. Since the sparse recovery 3D inversion method appears as the focusing phenomenon of inverse density, such density exceeds the range of the actual real anomaly source, thus, will not conform to the actual geological significance. For this reason, we must select the effective density constraint function that guarantees inversion results and that limits the inversion results within the physical, geophysical, and geological significance. Moreover, the density constraint function aims to determine the upper and lower limits of the density (m_b and m_a), so as to ensure that the residual density value of inversion change is within this range. Several density constraint functions exist, the first application of which was in conductivity inversion; for example, in 1999, Kim et al. (1999) used the logarithmic function of conductivity to constrain the varied electrical conductivity values within the reasonable range. This was succeeded by gravity and magnetic inversion application conducted by Portniaguine and Zhdanov (1999; 2002) for an aggregation process. A number of constraint functions have continued to appear in different studies and applications afterwards such as in the successful electrical resistivity tomography by Cardarelli and Fischanger (2006), and in the inverse hyperbolic tangent transfer function, aside from a previous logarithmic transformation, by Commer and Newman (2008), which limited the conductivity parameter in a transformation with the unbounded domain, and ensured rationality of the conductivity.

With regards to sparse inversion method, we referred to research and tests of various density constraint functions, and found that the simple upper and lower bound function is the most effective method for the study of the density function. Thus, in this work, we exploited the upper and lower function as the constraint function in the inversion as it is presumed to make the exceeding density of the inversion results fall within the reasonable range of the geological data, and to enable us to obtain inversion results that are consistent with the geological area. The specific upper and lower constraint function is given by

$$\begin{cases} m_i = m_b, & m_b < m_i \\ m_i = m_i & m_a < m_i < m_b, \\ m_i = m_a & m_i < m_a \end{cases} \quad i = 1, 2, ..., M, \qquad (18)$$

where m_b and m_a are the respective upper and lower bounds of the density. This constraint function is combined with the spare recovery method proposed in this paper to produce accurate, stable, and true inversion results.

Theory and model tests

In this section, we verified the effectiveness and feasibility of the proposed inversion method through tests employing two discrete models. The study area was a 1500 m × 1500 m square area, wherein the points and lines were separated from each other by 50 m. We used a discrete data grid point of 30×30, and dispersed the subsurface space of research area by dividing it into 30×30×15 grids. Each grid prim was a cube measuring 50 m × 50 m × 50 m. The number of ground observation points and the number of underground grids were consistent in each test.

Vertical rectangular model

The subsurface space has 16500 grids; Table 1 shows the spatial coordinates of the two models. The density contrast of each anomalous body is 1g/cm^3; the simulated values of gravity anomalies (data contained by Gauss noise 5%) are shown in Figure 2. The spatial distributions of models are shown in Figures 3a and 3b, where the characteristics of models can be clearly observed. As shown, the test region of the simulated values of gravity anomalies can cover the anomalous body completely, ensuring that the model of subsurface inversions can be obtained successfully.

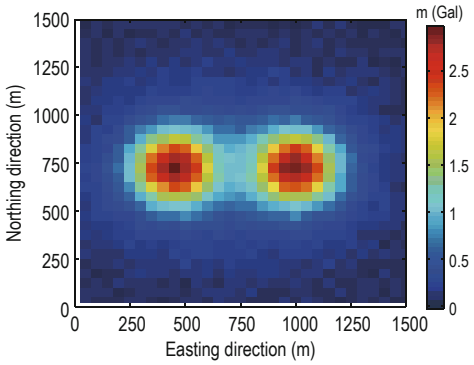

Fig.2 Gravity anomaly of adjacent rectangular anomaly.
(Gravity data contaminated by 5% Gauss noise)

Table 1 Spatial distribution characteristics of forward models of adjacent rectangular anomalies.

Model number	Easting direction (m) × northing direction (m) × depth direction (m)	Center position (m)	Density (g/cm^3)
A	250 m × 250 m × 200 m	475 × 775 × 300	1
B	250 m × 250 m × 200 m	1025 × 775 × 300	1

Applying 3D gravity inversion based on the iterative solution of sparse recovery with approximate zero norms, inversion calculations were carried out by the ground gravity data using the theoretical models. The objective function was established by the sensitivity matrix of model space and the gravity anomaly. Assuming that there was no *a priori* information, the initial model had zero vectors. In the inversion, ρ = 0.8, and σ is twice the results of the initial inversion. After constructing the objective function, we constrained the density of inversion results within 0.0–1 g/cm^3, and the final inversion results were obtained. Figure 3 shows the final results.

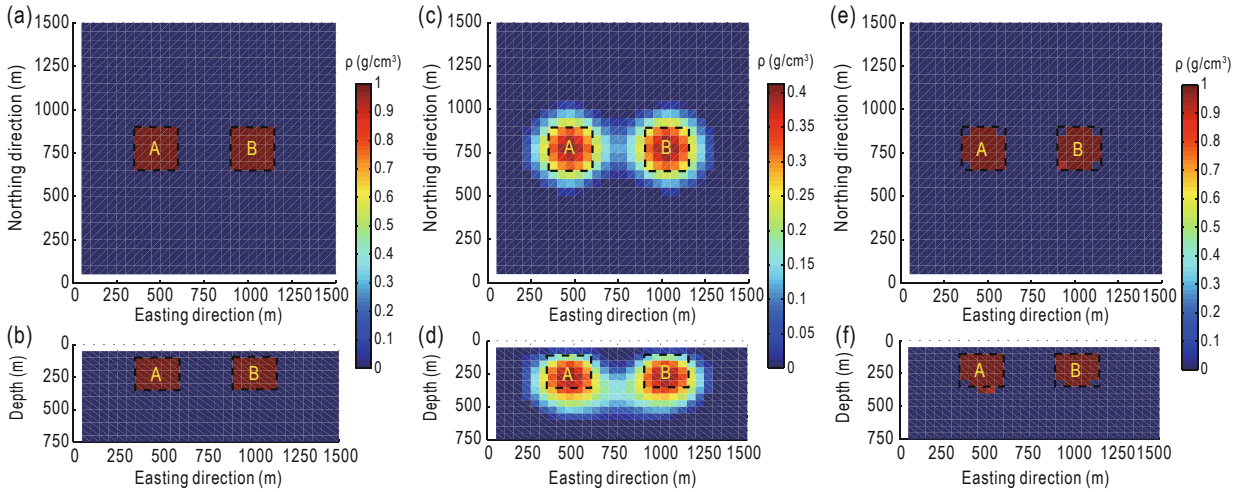

Fig.3 Comparative analysis of the inversion results and true models of two rectangular bodies.
(a) Section figure of true models in the depth of 250 m; (b) section figure of true models in the northing direction of 750 m; (c) section figure of inversion results in the depth of 250 m and; (d) section figure of inversion results in the northing direction of 750 m.

Based on the comparison (Figure 3) between the section figures of the inversion results and theoretical models, there good agreement in the depth of 250 m, where accurate density distribution and the boundary of subsurface anomalous bodies are clearly. In the northing direction of 750 m, a very small deviation between the inversion results and design models in the inversion results could be seen. At deep position, the inversion results vary slightly with those of the real model. Thus, inversion results show that the proposed inversion method can identify density distribution and spatial distribution characteristics of the subsurface anomalies very well. This paper adopted the MATLAB platform based on the 2G memory (CPU 2.1GHz) of the common

computer to finish the calculation. The time required to finish the inversion was 401.65 s. Based on the inversion results and the time requirement, the inversion method had very high accuracy level and vertical resolution.

Anomalous body model of inclined rock vein

As mentioned above, there are 16500 in the subsurface space; the spatial coordinates of the model body are shown in Table 2. The density contrast of the anomalous body is 1g/cm^3. Figure 4 shows the simulated values of gravity anomalies (Gauss noise containing 5%), while Figs. 5a and 5b show the spatial distribution of the model. Simulation of the gravity model anomaly values was completely contained in the inversion region. Based on the calculations, the subsurface model can be successfully obtained with the proposed inversion method.

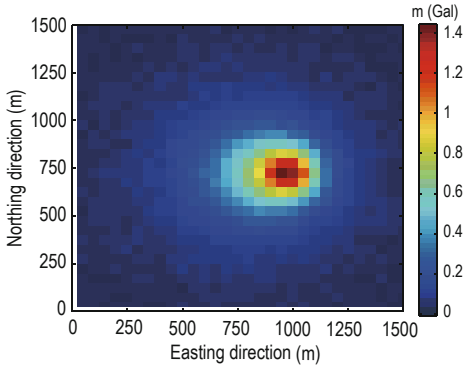

Fig.4 Gravity anomaly calculated by the forward model of the inclined rock vein.
(Anomalous gravity data contaminated by 5% Gauss noise).

Table 2 Spatial distribution characteristics of the forward model of the inclined rock vein

Model number	Easting direction (m) × northing direction (m) × depth direction (m)	Inclination	Center position (m)	Density (g/cm^3)
Dyke	150 m × 150 m × 400 m	135°	775 × 775 × 300	1

Using the method of 3D gravity inversion based on the iterative solution of the sparse recovery with approximate zero norms, we carried out the inversion calculation of the gravity anomaly produced by the theoretical model in the ground. We established the objective function using the sensitivity matrix of the model space and the gravity anomaly of the forward model. In the case without any priori information, the initial model vector is the zero vector. The initial value of the conjugate gradient method was treated as the first inversion results, which was subsequently used as the initial value for the succeeding inversion, where $\rho = 0.9$ (according to the characteristics of inversion anomaly, and its convergence with the iterative inversion method) and σ is twice the maximum value of the initial inversion solutions, so that the objective function is constructed. Densities of the inversion were constrained within 0–1g/cm^3, then the final results were obtained.

Inversion results for the inclined rock veins are shown in Figure 5.

Based on the comparison in Figure 5, in the depth of 250 m, the inversion results approximated the theoretical

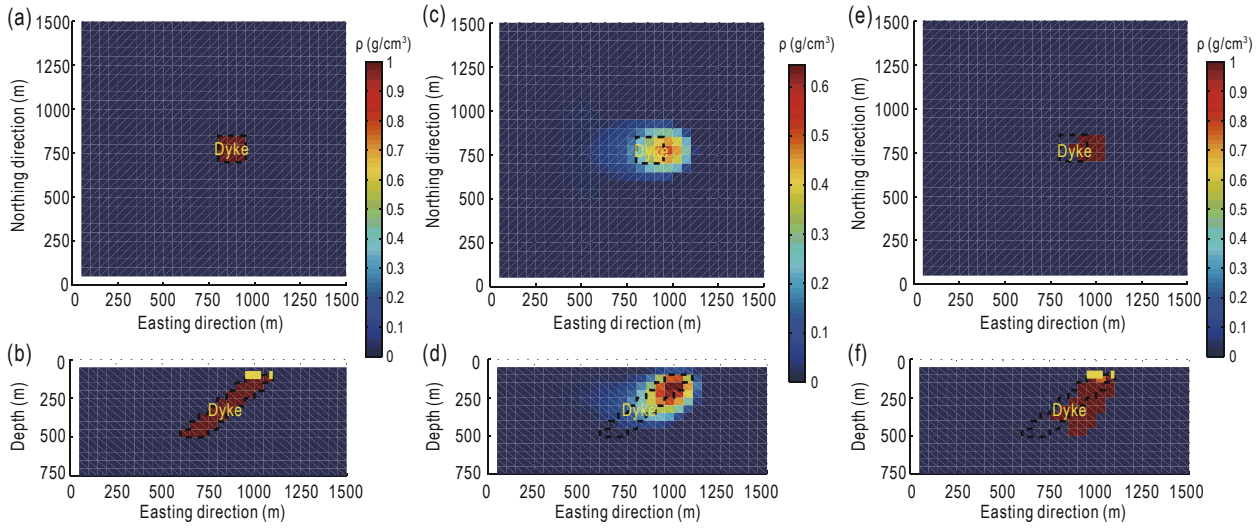

Fig.5 Three directions for the slice figure of the inclined rock vein.
(a) Section figure of true model in the depth of 250 m; (b) Section figure of true model in the northing direction of 750 m; (c) Section figure of inversion result in the depth of 250 m and; (d) Section figure of inversion result in the northing direction of 750 m.

model, and the horizontal position of the rock vein were approximately found. A certain deviation was observed but could be neglected as the information of anomalous boundaries obtained by the inversion was relatively accurate. Moreover, the density contrasts of the inversion results were in accordance with the true density contrasts. From the horizontal slices of the inversion research of the rock vein, the inversion method could obtain the characteristics of the shallow anomaly. From the compared results of the northing–southing direction slice, the approximate features of the rock vein could also be obtained, and the characteristics of the shallow region were very good. In contrast, inversion results in the deep region of the rock vein were relatively poor, which could be attributed to the less deep information of the gravity potential field data. In the inversion with less priori information, although the position of deep rock vein cannot be simulated, the approximate shape of the rock vein was clear. Moreover, the spatial distribution and density distribution of the rock vein were consistent with the model of the real setting, and inversion results were accurate as well. The inclined rock vein simulation was based on the MATLAB platform, and the results were calculated by an ordinary computer with a typical memory (2G CPU 2.1GHz). Inversion times were relatively longer, at 1042 s, than in the inversion of two separate rectangular anomalies, as these were decided by the models characteristics. Results proved the efficiency of the proposed 3D inversion method.

From the analysis of the inversion results of the theoretical model, the stabilized convergence adopting the approximate zero norm sparse recovery method was reached, with accurate inversion results, which were in good accord with the accuracy of data fitting. These results positively reflect those of the true model of the spatial density distribution. Moreover, this inversion process did not produce excess structural information of false interpretation and false results. Thus, the characteristics of the results were in accordance with the requirement of the most basic density distribution and structural features, which we mainly wanted to obtain. The results have very clear boundary information and accurate exception to the density values. Therefore, these characteristics meet the basic requirements of actual geophysical field data interpretation, researches, and empirical observations.

Application of real gravity data

The 3D inversion method can be applied to the inversion of an actual gravity data observation. The research region, located in the American state of Texas, was covered in rock salt. Due to the great relationship of oil and gas storage with rock salt, the results of this research is greatly significant for rock salt regions. In the actual initial iteration process of gravity inversion, a large σ avoid inversion solutions getting trapped into the local minima, making the results unstable. At this point, ρ values are relatively close to 1, which can prevent rapid inversion decay. To achieve relative stability of the inversion results, reducing ρ should be gradual. Depending on the rate of decrease, ρ can accelerate decrease in the speed of σ, thus, a final global minimal solution can be obtained as the gravity inversion result. In the real data inversion, the choice of ρ and σ is very important; thus, we set $\rho = 0.9$ for in this paper.

The actual survey region measures 16500 m × 16500 m. From Figure 6 of residual gravity anomaly, a low gravity anomaly was apparent in the region, as indicated by the grid of gravity data. The sub-surface region was divided into 33 × 33 × 10 vertical rectangular prisms, with geometry measuring 500 m × 500 m × 500 m.

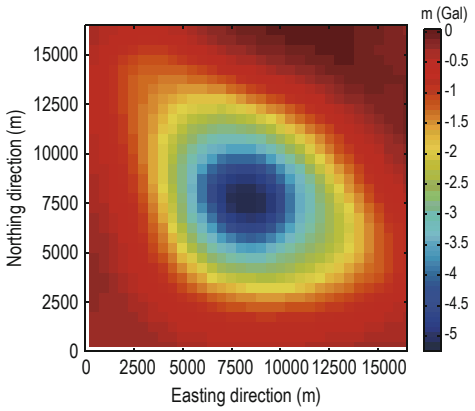

Fig.6 Real gravity data for the anomalous study region.

The real gravity data observed in the region was applied on the proposed 3D inversion. Density contrast distribution and variation characteristics of the sub-surface anomalies were obtained using the source characteristics, including the depth, north–south and east–west directions, of the geological structures. Afterwards, 3D models were constructed to show the sub-surface anomalous characteristics clearly. Figures 7 and 8 show the inversion results.

From the 3D inversion results of the gravity data observed, we found an obvious body with low density contrast in the study region. Based on the range of geological conditions and variations, the inversion body was salt rock with low density contrast. From the spatial

distribution of inverse target anomaly, the low density rock had approximate spheroidal geometry; its density range was within −0.2633–0 g/cm^3, which agreed with the real geological information. Figures 6 and 7 show the characteristics of depth variation of the sub-surface low density salt rock at an overall distribution range of 2500–5000 m, with the anomaly center depth of 4200 m. Since 3D inversion researches are relatively less on this region, depth inversion results of gravity and analysis results of logging data could be used to demonstrate and further illustrate the accuracy of our inversion method.

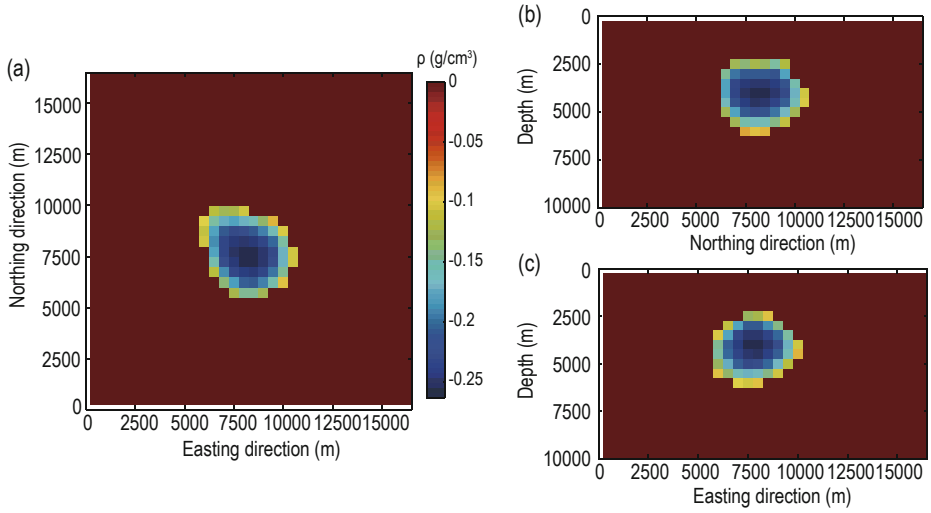

Fig.7 Inversion results of gravity data in the research region.
(a) Horizontal slice of the inversion results at the depth of 400 m; (b) Vertical slice of the inversion results at the northing direction of 800 m and; (c) vertical slice of the inversion results at the easting direction of 800 m.

From the comparison between 3D inversion results of gravity data and the previous results, the salt rock center depth of 3D inversion results was 4200 m. This is consistent with the results obtained by Salem, Essa, Qruc, and Ma et al. (Table 3), and thus, this method is applicable in real scenarios (Salem et al., 2004; Essa, 2007; Oru, 2010; Ma et al., 2012). Simultaneously, the previous logging test in the region yielded a center depth for the salt rock of nearly 4400 m, which agreed well with the result of our inversion method.

Based on the 3D visual figure in Figure 8, the shape of the low density dome was sphere-like, which is consistent with the assumption of previous researchers.

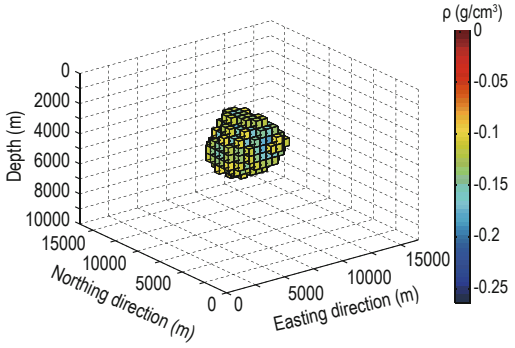

Fig.8 3D visual figure of the inversion results.

Table 3 Results of previous studies

Methods	Center depth (km)
Nettleton (1976)	4.97
Mohan et al. (1986)	4.63
Abdelrahman et al. (1991)	4.65
Shaw and Agarwal (1997)	4.13
Salem et al. (2004)	5.12 0.28
Essa (2007)	4.18
Qruc (2010)	4.12
Ma (2012)	4.14

Conclusions

The novel gravity inversion method was inspired by the approximate zero norm sparse recovery method, whose norm function replaced the model objective function in the conventional gravity data inversion. Lagrange method was employed for deduction of formulas to derive the corresponding inversion method. Moreover, the steepest descent method was applied to obtain the accurate geophysical inversion results. The main characteristics of this 3D inversion method are as follows: (1) The inversion algorithm mainly utilized the steepest descent and gradient projection

methods. During the inversion process, GG^T (forward) and its inverse matrix only needed to be calculated once to reduce the lengthy time requirement for the inversion, and to enhance the method's efficiency. (2) The algorithm employed the approximate zero norm objective model function. The obtained sparse feature could give sub-surface abnormal target source with clear spatial distribution and accurate density range. (3) In the approximate zero norm, the choice of the value of the parameters ρ and σ ensures that inversion results converge to the global minimum solution, not get trapped into the local minima.

Furthermore, the model test of gravity inversion achieved good results, displaying high resolution feature. The spatial features of the source and target anomaly density variations were consistent in the model test, which demonstrates the ability of the proposed 3D gravity inversion method to accurately obtain geometry and density distributions of sub-surface anomalies. When the inversion method was applied to the interpretation of gravity anomalies in Texas salt dome, it produced results that were consistent with those of the previous studies, such as the coincident geometry of the salt rock in the region; this finding can provide clues for oil and gas explorations in the area. These results prove the effectiveness of the inversion method in practical applications, and offer future studies on the geological formation of salt dome in the area.

Acknowledgments

The authors would like to thank reviewers Profs. Yao Changli, Jiang Puyu, and Luo Zhicai for their valuable comments and suggestions for the final paper, and also would like to extend their sincere thanks to Li Fengting, Geng Meixia, Qin Pengbo, et al. for the support of this research.

References

Abdelrahman, E. M., 1991, A least-squares minimization approach to invert gravity data: Geophysics, **56**(1), 115–118.

Barbosa, V. C. F., and Silva, J. B., 1994, Generalized compact gravity inversion: Geophysics, **59**(1), 57–68.

Bertete-Aguirre, H., Cherkaev, E., and Oristaglio, M., 2002, Non-smooth gravity problem with total variation penalization functional: Geophysical Journal International, **149**(2), 499–507.

Blakely, R. J., 1996, Potential theory in gravity and magnetic applications: Cambridge University Press.

Bijani, R., Ponteneto, C. F., Carlos, D. U., and Silva Dias, F. J. S., 2015, Three-dimensional gravity inversion using graph theory to delineate the skeleton of homogeneous sources. Geophysics, **80**(2), G53–G66.

Candes, E. J., and Tao, T., 2005, Decoding by linear programming: IEEE Transactions on, Information Theory, **51**(12), 4203–4215.

Cardarelli, E., and Fischanger, F., 2006, 2d data modelling by electrical resistivity tomography for complex subsurface geology: Geophysical Prospecting, **54**(2), 121–133.

Chen, S. S., Donoho, D. L., and Saunders, M. A., 1998, Atomic decomposition by basis pursuit: SIAM J. Sci. Comput., **20**(1), 33–61.

Chen, S., Saunders, M. A., and Donoho, D. L., 2001, Atomic decomposition by basis pursuit. Siam Review, **43**(1), 129–159.

Chen, G. X., Chen, S. C., and Wang, H. C., 2013, Geophysical data sparse reconstruction based on l0-norm minimization: Applied Geophysics, **10**(2), 181–190.

Chen, G. X., and Chen, S. C., 2014, Based on Lp norm sparse constrained regularization method of reconstruction of potential field data: Journal of Zhejiang University (Engineering Science) (4), 748–785.

Cheng, X. L., Zheng, X., and Han, W. M., 2013, the sparse algorithm to solve the underdetermined linear equations: Applied Mathematics A Journal of Chinese Universities, No. 2, 235–248.

Commer, M., 2011, Three-dimensional gravity modelling and focusing inversion using rectangular meshes: Geophysical Prospecting, **59**(5), 966–979.

Commer, M., and Newman, G. A., 2008, New advances in three-dimensional controlled-source electromagnetic inversion: Geophysical Journal International, **172**(2), 513–535.

Donoho, D. L., 2006, High-dimensional centrally symmetric polytopes with neighborliness proportional to dimension: Discrete & Computational Geometry, **35**(4), 617–652.

Donoho and David L., 2006, For most large underdetermined systems of linear equations the minimal $lsb 1$-norm solution is also the sparsest solution. Comm: Pure Appl. Math, **59**, 797–829.

Elad, M., 2007, Optimized projections for compressed sensing. IEEE Transactions on Signal Processing, **55**(12), 5695–5702.

Essa, K. S., 2007, Gravity data interpretation using the s-curves method: Journal of Geophysics and Engineering, **4**(2), 204.

Farquharson, C. G., 2008, Constructing piecewise-constant models in multidimensional minimum-structure inversions: Geophysics, **73**(1), K1–K9.

Fregoso, E., and Gallardo, L. A., 2009, Cross-gradients joint 3D inversion with applications to gravity and magnetic data: Geophysics, **74**(4), L31–L42.

Figueiredo, M. A., Nowak, R. D., and Wright, S. J. 2007,

Gradient projection for sparse reconstruction: Application to compressed sensing and other inverse problems: IEEE Journal of Selected Topics in Signal processing, **1**(4), 586–597.

Ghalehnoee, M. H., Ansari, A., and Ghorbani, A., 2017, Improving compact gravity inversion using new weighting functions: Geophysical Journal International, **208**(2), 546–560.

Gholami, A., and Siahkoohi, H. R., 2010, Regularization of linear and non-linear geophysical ill-posed problems with joint sparsity constraints: Geophysical Journal International, **180**(2), 871–882.

Guillen, A., and Menichetti, V., 1984, Gravity and magnetic inversion with minimization of a specific functional: Geophysics, **49**(8), 1354–1360.

Kim, H. J., Song, Y., & Lee, K. H., 1999, Inequality constraint in least-squares inversion of geophysical data: Earth Planets & Space, **51**(4), 255–259.

Last, B. J., and Kubik, K., 1983, Compact gravity inversion: Geophysics, **48**(48), 713–721.

Lelièvre, P. G., and Oldenburg, D. W., 2009, A comprehensive study of including structural orientation information in geophysical inversions: Geophysical Journal International, **178**(178), 623–637.

Li, Y., and Oldenburg, D. W., 1996, 3-D inversion of magnetic data: Geophysics, **61**(2), 394–408.

Li, Y., and Oldenburg, D. W., 1998, 3-D inversion of gravity data: Geophysics, **63**(1), 109–119.

Li, Y., Cichocki, A., and Amari, S. I., 2003, Sparse component analysis for blind source separation with less sensors than sources: Independent Component Analysis, 89–94.

Ma, G. Q., Du, X. J., and Li, L. L., 2012, Comparison of the tensor local wavenumber method with the conventional local wavenumber method for interpretation of total tensor data of potential fields: Chinese Journal of Geophysics, **55**(7), 2450–2461.

Mallat, S. G., and Zhang, Z., 1993, Matching pursuits with time-frequency dictionaries: IEEE Transactions on Signal Processing, **41**(12), 3397–3415.

Mohan, N. L., Anandababu, L., and Rao, S. V. S., 1986, Gravity interpretation using the mellin transform: Digital Library Home, **51**(1), 114–122.

Mohimani, H., Babaie-Zadeh, M., & Jutten, C., 2009, A fast approach for overcomplete sparse decomposition based on smoothed l0, norm: IEEE Press.

Nettleton, L. L., 1976, Gravity and magnetics in oil prospecting. McGraw-Hill Companies.

Oruç, B., 2010, Location and depth estimation of point-dipole and line of dipoles using analytic signals of the magnetic gradient tensor and magnitude of vector components: Journal of Applied Geophysics, **70**(1), 27–37.

Portniaguine, O., and Zhdanov, M. S., 1999, Focusing geophysical inversion images: Geophysics, **64**(3), 874.

Portniaguine, O., and Zhdanov, M. S., 2002, 3-D magnetic inversion with data compression and image focusing: Geophysics, **67**(5), 1532–1541.

Qi, G., Lv, Q. T., Yan, J. Y., Wu, M. A., and Liu, Y., 2012, Geologic constrained 3D gravity and magnetic modeling of Nihe Deposit-A case study: Chinese Journal of Geophysics, **55**(12), 4194–4206.

Salem, A., Ravat, D., Mushayandebvu, M. F., and Ushijima, K., 2004, Linearized least-squares method for interpretation of potential-field data from sources of simple geometry: Geophysics, **69**(3), 783–788.

Shaw, R. K., and Agarwal, B. N. P., 1997, A generalized concept of resultant gradient to interpret potential field maps: Geophysical Prospecting, **45**(6), 1003–1011.

Silva Dias, F. J. S., Barbosa, V. C., and Silva, J. B. C., 2009, 3D gravity inversion through an adaptive-learning procedure: Geophysics, **74**(3), I9–I21.

Silva Dias, F. J. S., Barbosa, V. C. F., and Silva, J. B. C., 2011, Adaptive learning 3d gravity inversion for salt-body imaging: Geophysics, **76**(3), 149–157.

Silva, J. B. C., and Barbosa, V. C. F., 2006, Gravity inversion of basement relief and estimation of density contrast variation with depth: Geophysics, **71**, J51–J58.

Tontini, F. C., Cocchi, L., and Carmisciano, C., 2009, Rapid 3-D forward model of potential fields with application to the Palinuro Seamount magnetic anomaly (southern Tyrrhenian Sea, Italy): Journal of Geophysical Research: Solid Earth, **114**(B2).

Tontini, F., Ronde, C. E. J., Yoerger, D., Kinsey, J., and Tivey, M., 2012, 3-D focused inversion of near-seafloor magnetic data with application to the Brothers volcano hydrothermal system, Southern Pacific Ocean, New Zealand: Journal of Geophysical Research: Solid Earth, **117**(B10).

Wang, T. H., Huang, D. N., Ma, G. Q., Meng, Z. H., and Li, Y., 2017, Improved preconditioned conjugate gradient algorithm and application in 3D inversion of gravity-gradiometry data: Applied Geophysics, **14**(2), 301–313.

Zhang, Y., Wu, Y., Yan, J., Wang, H., Rodriguez, J. A. P., and Qiu, Y., 2018, 3d inversion of full gravity gradient tensor data in spherical coordinate system using local north-oriented frame: Earth Planets & Space, **70**(1), 58.

Zhdanov, M. S., Ellis, R., and Mukherjee, S., 2004, Three-dimensional regularized focusing inversion of gravity gradient tensor component data: Geophysics, **69**(4), 925–937.

Meng Zhao-Hai, Engineer, received his B.S. (2011) in Geophysics at the College of Geo-Exploration Science and Technology, Jilin University, and received his Ph.D (2016). in petrology, mineralogy, and geology at the College of Earth Science, Jilin University. He is currently working in Tianjin Navigation Instrument Research Institute, and his major research interests are geophysical instrumentation development and geophysical data processing.